Armcx1 Alleviates Secondary Brain Injury After Traumatic Brain Injury by Reducing Apoptosis and Axonal Injury in a Mouse Model of Controlled Cortical Impact

Dengfeng Lu
First Affiliated Hospital of Soochow University
Yi Wang
First Affiliated Hospital of Soochow University
Guangjie Liu
First Affiliated Hospital of Soochow University
Shixin Wang
First Affiliated Hospital of Soochow University
Jing Wang
First Affiliated Hospital of Soochow University
Xiaoou Sun (sunxo76@163.com)
First Affiliated Hospital of Soochow University https://orcid.org/0000-0002-1839-4242
Yu Wu
First Affiliated Hospital of Soochow University

Research Article

Keywords: Armcx1, traumatic brain injury, miR-223-3P, mitochondrial transport, apoptosis, axonal injury

Posted Date: November 30th, 2021

DOI: https://doi.org/10.21203/rs.3.rs-1100916/v1

Abstract

Armcx1 is highly expressed in the brain and is located in the mitochondrial outer membrane of neurons, where it mediates mitochondrial transport. Mitochondrial transport promotes the removal of damaged mitochondria and the replenishment of healthy mitochondria, which are essential for neuronal survival after traumatic brain injury (TBI). This study investigated the role of Armcx1 and its underlying regulator(s) in secondary brain injury (SBI) after TBI. An in vivo TBI model was established in C57BL/6 mice via controlled cortical impact (CCI). Adeno-associated viruses with Armcx1 overexpression and knockdown were constructed and administered to mice by stereotactic cortical injection. Exogenous miR-223-3P mimic or inhibitor was transfected into cultured cortical neurons, which were then scratched to simulate TBI in vitro. The Armcx1 protein level was found to be decreased in peri-lesion tissue, particularly in neurons. The overexpression of Armcx1 significantly reduced TBI-induced neurological dysfunction, apoptosis, axonal injury, and mitochondrial dysfunction, while knockdown of Armcx1 had the opposite effect. Armcx1 was a direct target of miR-223-3P. The miR-223-3P mimic significantly reduced the Armcx1 protein level, while the miR-223-3P inhibitor had the opposite effect. Finally, the miR-223-3P inhibitor significantly improved mitochondrial membrane potential and increased the total length of the neurites without affecting branching numbers, while the miR-223-3P mimic had the opposite effect. In summary, our results suggest that the decreased expression of Armcx1 protein in neurons after experimental TBI aggravates secondary brain injury, which may be regulated by miR-223-3P. Therefore, this study provides a potential therapeutic approach for treating TBI.

Introduction

Traumatic brain injury (TBI) is a common trauma with a high incidence in both children and adults. Common causes include traffic accidents, sports injuries, and accidents on construction sites and during military operations. With advances in neurosurgical techniques, the mortality rate of patients with TBI has decreased significantly. However, there has been no significant decrease in the rate of disability among survivors, who are often accompanied by impairment of consciousness, speech, physical activity, mental and emotional disorders, and other sequelae, which seriously affect their quality of life[1, 2]. TBI is a complex pathophysiological process that can be divided into two stages: primary injury and secondary injury[3]. Primary injuries are directly caused by mechanical forces that exceed the structural limits of cell and tissue and occur at the moment of mechanical impact, resulting in nonspecific cell loss, diffuse axonal injury, and intracranial hemorrhage[4]. Secondary injury is a progressive pathological process involving oxidative stress, inflammation, mitochondrial dysfunction, and secondary axonal injury and apoptosis, which occurs minutes after mechanical impact and lasts for several days[5]. Primary brain damage is uncontrollable and incurable. In contrast, the occurrence of secondary brain injury is relatively slow and leads to destruction of the blood-brain barrier, brain edema, and neurobehavioral disorders, which seriously affect the prognosis of patients with TBI. Therefore, it is particularly important to study the key factors regulating secondary nerve injury after TBI and to find new targets for improving the prognosis of patients with TBI.

Mitochondria are the energy factories of cells, and play a central role in metabolism and biological energy conversion. More than 90% of the energy required by neurons to function properly is supplied by ATP produced by mitochondrial metabolism. As an important semi-autonomous organelle, mitochondrial DNA (mtDNA) is extremely vulnerable to reactive oxygen species (ROS) attack and mutation. Many human diseases, including Alzheimer's disease, premature aging, Huntington's disease, Parkinson's disease, cancer, diabetes, and epilepsy, are associated with mitochondrial dysfunction. Previous studies and our previous data indicate that mitochondrial dysfunction exists in neurons after TBI[6, 7]. In neurons after TBI, damaged mitochondria are transported to the soma and cleaned by autophagy and other methods, while healthy mitochondria are transported to the damaged site to provide energy, which is key to nerve function repair. Therefore, analyzing the mitochondrial transport of neurons and exploring the key factors that regulate the mitochondrial transport of neurons after TBI will provide new ideas for the effective prevention and treatment of nerve injury after TBI.

As energy-intensive brain cells, neurons are rich in mitochondria in both the soma and neurites and also have strict requirements for the function of mitochondria[8]. Previous studies have shown that the loss of mitochondria at the axon terminal leads to synaptic transmission disorders[9–11]. Our previous data showed that damaged mitochondria were present in the soma and axon of neurons after TBI. Removing damaged mitochondria and replenishing healthy mitochondria are key to maintaining normal neuronal function[12]. Damaged mitochondria need to be transported to the cell body for degradation, and mitochondrial regeneration mainly occurs in the soma. Thus, both the removal of damaged mitochondria and the replenishment of healthy mitochondria depend on mitochondrial transport. During the early stage of neuronal development, mitochondrial transport within the neuron is active to ensure various energy needs are met. During development, mitochondria in neurons tend to solidify, and in mature neurons, approximately 70% of the mitochondria are immobilized. The phenomenon of mitochondrial transport solidification partly explains why adult neurons are difficult to reshape and regenerate after injury. Recently, neuronal mitochondrial transport has attracted much attention, and neuronal mitochondrial transport disorders have been found to be associated with a variety of neurological diseases[13–17]. Therefore, after TBI, the enhancement of neuronal mitochondrial transport may be beneficial to alleviate secondary brain injury.

The Armadillo Repeat Containing, X-Linked 1 (Armcx1) is a member of a poorly characterized cluster of six genes unique to placental mammals, which regulate protein-protein interaction involved in nuclear transport, cellular connection, and transcription activation. Also known as ALEX1, Armcx1 consists of a N-terminal transmembrane domain, a mitochondrial targeted sequence, a nuclear localization signal, and several Arm-like repeat domains. Armcx1 is a mammalian-specific protein, which is highly expressed in the brain[18]. Romain et al. (2016) found that Armcx1 is located in the mitochondria of neurons. Overexpression of Armcx1 can promote the survival of neurons and the repair of damaged axons by enhancing mitochondrial transport in adult retinal ganglion cells. In contrast, knockout of Armcx1 increased neuronal death and axonal damage[18].

MicroRNAs are a class of small non-coding RNAs, which are between 20 and 23 nucleotides in length. MicroRNAs regulate physiological and pathological processes mainly through interacting with the 3'-UTR of the targeted mRNA, leading to mRNA degradation and/or translational inhibition[19]. MiR-223-3P is a hematopoietic-related miRNA that regulates myeloid and granulocyte differentiation and dendritic cell activation, and also affects the inflammatory response[20]. It has been reported that miR-223-3P is also expressed at a certain level in the brain, especially in the cerebral cortex and hippocampus, and the expression level is increased in the brain after TBI[21–23]. This study aimed to explore the roles and mechanisms of Armcx1 and miR-223-3P in in vitro and in vivo models of TBI.

Materials And Methods

Experimental animals

Adult male C57BL/6 mice (21 g–28 g) were provided by the Animal Center of Chinese Academy of Sciences (Shanghai, China). All procedures were approved by the Institutional Animal Care Committee of the Soochow University and complied with the ARRIVE (Animal Research: Reporting In Vivo Experiments) guidelines. All animals were housed in a quiet and comfortable environment (temperature: 18–22°C, relative humidity: 40%–50%), with a 12 h light/dark cycle. Animals had free access to food and water. Sample numbers were determined by power analysis during the animal ethics dossier application.

Establishment of a controlled cortical impact mouse model

The operation was performed one week after the mice were housed. The TBI model was established by a precision percussion device (68099II, RWD, Shenzhen, China). In brief, mice were anesthetized with isoflurane (3% induction; 1.5% maintenance) and properly fixed in a stereotactic apparatus. A midline incision was made after disinfection to expose the skull. The anterior fontanel was set as the origin, and a coordinate of (2 mm, –2 mm) was set as the center site of craniotomy and impact. An electric drill was used to perform the craniotomy, generating a 3 mm-diameter skull flap, which was removed. During this process, mice with damaged dura were excluded from the experiment. Subsequently, a circular impact tip with a diameter of 2 mm was used to vertically hit the dura mater surface with the following parameters: velocity of 4.5 m/s, depth of 1.0 mm, and duration of 100 ms, resulting in a moderate controlled cortical impact (CCI). Then, the bone flap was returned and the scalp was sutured. The sham operation group received craniotomy, but did not undergo CCI injury. The coronal sections of the brain tissue of the sham group and CCI group are shown in Fig. 1a. The mice were then transferred to the cage and allowed to recover fully from anesthesia (as exhibited by resumption of movement and grooming). During the operation, a 37°C constant heating pad was used to maintain the body temperature of mice.

Neuron culture

As mentioned previously, primary cortical neurons (PCNs) from E17 C57BL/6 mouse embryos were isolated and cultured[24]. Briefly, the embryonic mouse brains were removed with sterilized instruments after the pregnant mice were executed. The meninges and blood vessels were removed from the brains of

embryonic mice. The bilateral cerebral cortex was taken and the rest of the brain tissue was discarded. The cortical tissue was then digested with 0.25% trypsin-EDTA solution (Gibco, Carlsbad, CA, USA) for 5–8 min at 37°C. After digestion, the tissue was washed three times with phosphate buffered saline (PBS). Fetal bovine serum (FBS; from Gibco) was added to neutralize the trypsin; then, all fluids were filtered and any unfiltered tissue clumps were discarded. The remaining suspension was centrifuged at 1000 rpm/min for 5 min before discarding the supernatant and collecting the lower precipitate. The cell precipitate was resuspended in a tube containing neurobasal medium (from Gibco). The contents of the tube were mixed well to distribute the cells evenly. An appropriate resuspension volume was then drawn on the blood cell count plate and the number of neurons was counted using a microscope. The neurons were then plated onto culture dishes, 6-well plates, or 24-well plates (Corning, NY, USA) precoated with 0.1 mg/ml poly-D-lysine (Sigma-Aldrich, St. Louis, MO, USA) and cultured in fresh neurobasal medium containing 2% B27, 2 mM L-glutamine, 50 U/ml penicillin, and 50 U/ml streptomycin (all from Gibco). The dishes and plates were placed in a 37°C incubator containing 5% CO_2. Half of the medium was replaced with fresh medium every 2 days. After transfection and scratching, the neurons were harvested for the following experiments.

Establishment of an in vitro model of scratch injury

As described previously[25, 26], scratch injury, a widely accepted method, was used to establish an in vitro model of TBI. In brief, a sterile pipette tip (10 μl) was used to manually scratch the culture. In 6-well and 24-well plates, 12 × 12 and 6 × 6 scratches were generated, respectively, in each well, and 3 mm × 3 mm grids were formed. The neurons exposed to the tip died immediately, and those far away from the scratches underwent progressive secondary injury. The cells in the control group did not receive this intervention. The injured culture and the corresponding control group were placed in an incubator containing 5% CO_2 and humidified air at 37°C for 72 h.

Experimental grouping

Part 1: Time course analysis of the protein levels of Armcx1 after CCI

In experiment 1, 36 mice (40 in total; 36 survived the surgery) were randomly assigned to six groups with six mice per group. A sham group and five experimental groups were arranged according to the time points of 6 h, 1 d, 3 d, 5 d, and 7 d after CCI. At the specified time point after the surgery, all mice were killed and their brain tissues were collected for the subsequent immunoblotting and immunofluorescence experiments (Fig. 1b).

Part 2: Roles of Armcx1 in secondary brain injury after CCI and the underlying mechanisms in vivo

In this part, the knockdown effect of AAV was verified. Twenty-four mice (27; 3 were excluded) were randomly assigned to the following four groups: pAAV-hSYN-EGFP-miR30shRNA (NC), pAAV-hSYN-EGFP-miR30shRNA(Armcx1)-(1), pAAV-hSYN-EGFP-miR30shRNA(Armcx1)-(2), and pAAV-hSYN-EGFP-miR30shRNA(Armcx1)-(3), with 6 mice per group. Three weeks after injection of the virus, all of the mice

in all four groups were sacrificed, and the brain tissues were collected for western blot analysis to identify the virus group with a good knockdown effect for use in the following experiments. Then, 126 mice (136; 10 were excluded) were randomly assigned to the following six groups: sham group, CCI group, CCI + pAAV-hSYN-EGFP group, CCI + pAAV-hSYN-EGFP-Armcx1 group, CCI + pAAV-hSYN-EGFP-miR30shRNA (NC) group, and CCI + pAAV-hSYN-EGFP-miR30shRNA (Armcx1) group. The operation was performed 3 weeks after injection of the virus. The brains of six mice per group were extracted 72 h after CCI for use in western blot, immunofluorescence, and immunohistochemistry. Another three mice in each group were executed 72 h after CCI transmission electron microscopy (TEM), while the remaining 12 mice were examined for behavioral impairment in the week following surgery (Fig. 1c).

Part 3: Further exploration of the mechanism of miR-223-3P/Armcx1 in vitro

As shown in Fig. 1d, the cultured neurons were divided into the following six groups: control group, scratch group, mimic-NC group, mmu-miR-223-3P mimic group, inhibitor-NC group, and mmu-miR-223-3P inhibitor group. Transfection reagents were given 24 h before scratch injury. According to previous time course experiments, the cells were collected at 72 h after scratch injury for western blot, immunofluorescence, and JC-1 staining.

Antibodies

The antibody against Armcx1 (PA5-50911) was purchased from Invitrogen; the Armcx1 antibody (SAB2100153) was from Sigma Aldrich; the antibodies against cleaved caspase-9 (9507), β-actin (4970), and β3-tubulin (4466) were from Cell Signaling Technology; and the anti-NeuN antibody – a neuronal marker (ab104224), NeuN antibody (ab177487), GFAP antibody (ab134436), and Iba1 antibody (ab48004) were from Abcam. The secondary antibodies for western blotting, including goat anti-rabbit IgG-HRP (bs13278) and goat anti-mouse IgG-HRP (bs12478), were purchased from Bioworld. The secondary antibodies for immunofluorescence, including Alexa Fluor 488 donkey anti-rabbit IgG (H+L) highly cross-adsorbed secondary antibody (A21206), Alexa Fluor 555 goat anti-rabbit IgG (H+L) cross-adsorbed secondary antibody (A21428), Alexa Fluor 488 goat anti-mouse IgG (H+L) cross-adsorbed secondary antibody (A11001), Alexa Fluor 555 donkey anti-mouse IgG (H+L) highly cross-adsorbed secondary antibody (A31570), Alexa Fluor 555 goat anti-chicken IgY (H+L) secondary antibody (21437), Alexa Fluor Plus 555 donkey anti-goat IgG (H+L) highly cross-adsorbed secondary antibody (A32816), and Alexa Fluor 633 goat anti-rabbit IgG (H+L) cross-adsorbed secondary antibody (A-21070) were from Invitrogen.

Injection of the recombinant AAV vector in vivo

Overexpression and knockdown of Armcx1 were achieved by transfection of adeno-associated virus (AAV). To establish and maintain the specific regulation of Armcx1, AAV2/9-hSYN-EGFP-Armcx1 (over-Armcx1) and AAV2/9-hSYN-EGFP-miR30shRNA (Armcx1) (sh-Armcx1) were designed by OBiO (Shanghai,

China) and used to up- and down-regulate Armcx1 protein levels, respectively. There were three virus strains in the knockdown group, and the strain with the best knockdown effect was selected for further experiments. Meanwhile, the AAV2/9-hSYN-EGFP (over-NC) and AAV2/9-hSYN-EGFP-miR30shRNA(NC) (sh-NC) were used as the relative negative control. The Armcx1 shRNA sequence was 5'-GGAACAGGACAAGTGGGAA-3', 5'-CCAACATGACTGTAACTAA-3', and 5'-GGTGGTCAAAGTGAAAGTT-3'; the shRNA NC sequence was 5’-AGGAAGTCGTGAGAAGTAGAAT-3’. The experimental CCI was established on the 21st day after AAV injection. In brief, mice were anesthetized with isoflurane (3% induction; 1.5% maintenance) and fixed in an appropriate stereotactic frame. A midline scalp incision was made to expose the skull before injecting the virus suspension into the cortex of the mice (0.5 μl over 10 min per site, two sites per mouse). The syringe (Gaoge, Shanghai, China), fitted with a sharp-tip 30-gauge, was placed at the following coordinates: anterior-posterior (AP), bregma 0 mm; medio-lateral (ML), 2.0 mm over the right hemisphere; dorso-ventral (DV), 1.8 mm; bregma, 2.0 mm; medio-lateral (ML), 2.0 mm over the right hemisphere; and dorso-ventral (DV), 1.8 mm from the dura mater. The needle was gently retracted after 10 min to avoid a negative pressure-driven dispersion of the vector solution upward along the needle tract. At the end of the procedure, the scalp was sutured and the mice were allowed to recover on a heating pad maintained at 37°C.

Cell transfection

The mmu-miR-223-3P mimic, mmu-miR-223-3P inhibitor was purchased from RiboBio (Guangzhou, China). Transfection of PCNs was performed on the fifth day in 24-well plates in vitro (DIV). Cells were transfected with riboFECT^{TM} CP Reagent (RiboBio, Guangzhou, China) containing the mmu-miR-223-3P mimic, mmu-miR-223-3P inhibitor according to the supplier’s instructions. Twenty-four hours after transfection, the media was replaced with normal conditioned media, and the cells were scratched to establish in vitro model.

Western blot

In brief, the extracted cells or brain tissue samples around the contusion were collected, homogenized, and mechanically lysed in cold RIPA lysis buffer (Beyotime, Shanghai, China). The samples were then centrifuged for 10 min (4°C, 12000 g). The supernatant was immediately collected and the BCA Protein Assay Kit (Beyotime, Shanghai, China) was used to measure protein concentrations according to the manufacturer’s instructions. Equal amounts of protein samples were loaded onto SDS-polyacrylamide gel, separated, and electrophoretically transferred to a nitrocellulose membrane (Millikon, Spartanburg, SC, USA). Then, the membranes were blocked with 5% bovine serum albumin (BioSharp, Anhui, China) (at room temperature for 1 h), after which the membranes were incubated overnight with primary antibodies at 4°C. GAPDH was also detected and acted as a loading control. The second antibody, coupled with horseradish peroxidase (HRP), was then incubated with TBST for 2 h at room temperature to clean the membranes. The protein bands were displayed by an enhanced chemiluminescence (ECL) Kit (Beyotime, Shanghai, China), and the relative protein quantity was analyzed via ImageJ software (NIH, USA).

Immunofluorescence analysis

For in vivo experiments, the brain samples were fixed in 4% paraformaldehyde, embedded in paraffin, cut into 4 μm sections, and dewaxed immediately before immunofluorescence staining. For in vitro experiments, the cultured neurons were fixed in 4% paraformaldehyde. The sections and cells were then stained with primary antibodies and appropriate secondary antibodies. Nuclei were stained with DAPI mounting medium. Finally, the sections and cells were observed using a fluorescence microscope (Olympus, Tokyo, Japan). At least six random sections of each sample were examined, and the representative results are shown. The relative fluorescence intensity was analyzed using the ImageJ program.

Immunohistochemistry analysis

Paraffin-embedded brain sections were dewaxed with gradient ethanol and xylene, and then boiled in a microwave with citrate buffer for 30 min to retrieve antigens. After washing three times with PBS, the sections were incubated with 3% hydrogen peroxide and 3% bovine serum albumin (BSA; BioSharp, Anhui, China) to block endogenous peroxidase and nonspecific binding, respectively. Then, sections were incubated with primary antibodies against β-APP (51-2700, Invitrogen, Carlsbad, CA, USA) overnight at 4°C. The sections were then washed three times with PBS, before incubating with biotinylated secondary antibody in PBS containing 0.3% Triton X-100 for 1 h. Following three washes with PBS, the sections were overlaid with the avidin–biotin horseradish peroxidase (HRP) complex (Vector). Finally, 3,3'-diaminobenzidine solution (DAB; Zsgbbio, Beijing, China) was used to detect the HRP activity under light microscopy. ImageJ software was used to analyze the IHC images.

Transmission electron microscope

A transmission electron microscope (TEM) was used to observe the cortical ultrastructure 3 days after CCI. After the mice were anesthetized and killed, the cortical tissue around the contusion (approximately 1 × 2 mm^2) was quickly removed, immediately placed in 2.5% glutaraldehyde, and fixed at 40°C for 4 h. The tissues were rinsed with PBS three times for 10 min each, followed by fixation with 1% osmium acid at 40°C for 2 h. The tissues were rinsed a further three times with PBS buffer. The tissues were then dehydrated in a gradient of 30%, 50%, 70%, 90%, and 100% ethanol for 10 min each, then subject to a further dehydration in 100% ethanol. Subsequently, the samples were embedded with Epon812 epoxy resin and cured at 370°C, 450°C, and 650°C for 24 h each, followed by semi-thin section localization. Ultrathin sectioning was performed using an UltracutE Ultrathin slicer. Tissue was stained with lead uranium-dioxy nitrate acetate. The ultrastructure was observed using a JEM - 1200EX transmission electron microscope (JEOL, Tokyo, Japan).

JC-1 staining

The mitochondrial membrane potential assay kit with JC-1 (Beyotime, Shanghai, China) was used to detect changes in mitochondrial membrane potential (MMP), which can be used for early detection of cell

apoptosis. Tests were performed using the kit according to the manufacturer's instructions. The culture medium was removed from one well of the 24-well plate, and the cells were washed once with PBS before adding 300 μl cell culture medium. Subsequently, 300 μl JC-1 dyeing solution was added to each well and mixed well before incubating at 37°C for 20 min. Next, an appropriate volume of JC-1 staining buffer (1X) was prepared and placed on ice during incubation. The supernatant was then removed and the cells were washed twice with JC-1 staining buffer (1 X). Subsequently, 500 μl cell culture medium was added. The cells crawled over the slide and were immediately observed under fluorescence microscopy. The red fluorescent complex indicates a higher potential in the mitochondrial membrane. In cells with damaged mitochondria, JC-1 remains in its monomer form and displays green fluorescence. For quantitative analysis, three fields (40×) were randomly selected from three independent trials. The ratio of red to green fluorescence was measured and analyzed by ImageJ.

Neurobehavioral assessment

Modified neurological severity score (mNSS)

The mNSS test was performed to evaluate the neurological functional outcomes of mice. The mNSS test consists of ten tasks that can be used to evaluate the sensory, motor, balance, and reflex functions of mice. Neurological function was graded from 0 to 18, where 0 indicates normal function and 18 indicates maximal deficit. One point was awarded if the mice were unable to perform the test or lacked an expected reaction; thus, the higher the score, the more severe the injury. The mice were trained and assessed before surgery to ensure that the normal score was 0. Then, the tests were conducted blindly and the scores were recorded on days 3, 5, and 7 after CCI.

Rotarod test

The rotarod test was used to evaluate motor function after CCI, as described previously[27]. Briefly, mice were placed on an accelerated rotating rod, with the speed increasing linearly from 4 to 40 rpm within 2 min, and maintained for 3 min or until the mice dropped. Each mouse was tested twice a day, with a 15 min interval between tests. The latency to fall off the rotating rod was recorded. Passive rotation, or accompanying the rotating rod without walking, was also considered a fall. Data are expressed as the mean values of the two experiments. The mice were trained three times a day for 3 days before undergoing the operation. The mean value 1 day before the surgery was taken as the baseline. The test was repeated 3, 5, and 7 days after the surgery.

Adhesive removal test

The adhesive removal test was performed to assess the tactile responses and sensorimotor asymmetries of the mice. The sticking plaster (2 × 3 mm) was applied on the left paw (impaired side, contralateral to the brain lesion) as a tactile stimulus. This test was administered on pre-injury days 1, 2, and 3, and post-CCI days 3, 5, and 7. Two trials per day were administered 5 min apart to minimize habituation effects. The baseline latencies to contact and remove the tape were recorded before injury. Tactile responses were

measured by recording the time until the initial contact of the impaired forepaw with the mouth, as well as the time to remove the sticking plaster from the impaired forepaw using the mouth, with a maximum observation period of 120 s. The latency to contact and remove the sticking plaster from the left forelimb was the dependent variable of interest.

Statistical analysis

All data were statistically analyzed using GraphPad Prism 8.0.2 and are presented as the mean ± standard deviation (SD). The data sets in each group were tested for normality of distribution using the Shapiro–Wilk test. The two data groups with normal distributions were compared using the two-tailed unpaired Student's t-test, and the Mann–Whitney U test was used for the two non-normal data groups. Statistical comparisons between groups were performed using one- or two-way ANOVA and post hoc least significant difference tests for multiple comparisons. P-values < 0.05 were considered statistically significant.

Results

Endogenous expression level of Armcx1 decreased after CCI

To evaluate the expression of Armcx1 after CCI, the protein levels of Armcx1 were detected by western blot. The results showed that, compared to the sham group, the protein level of Armcx1 in the region of interest (ROI) (as shown in Fig. 2a) decreased gradually after CCI, reached its lowest level (decreased by approximately 50%) at 3 days, and then gradually rebounded (Fig. 2b and c). To further clarify the cell types expressing Armcx1, we detected the expression of Armcx1 in neurons, microglia, and astrocytes. Brain sections incubated with Armcx1 and NeuN (neuronal marker), iba1 (microglial marker), or GFAP (astrocytic marker) were used for dual immunofluorescence staining. The results showed that Armcx1 protein was mainly expressed in neurons, and rarely in microglia and astrocytes (Fig. 2d; Fig. S1a and b). Moreover, Armcx1 protein was expressed in neurons in both the sham group and CCI group. However, compared to the sham group, the expression level of Armcx1 in neurons after CCI was significantly decreased, which was consistent with our western blot results (Fig. 2d and e). Notably, Armcx1 was expressed in both the soma and axons of neurons in the sham group. However, the expression of Armcx1 was significantly decreased in the CCI group, especially in axons. Hence, we focused on Armcx1 in axons.

Overexpression of Armcx1 improved the neurobehavioral performance of CCI mice, which was impeded by Armcx1 knockdown

To elucidate the effects of changes in the expression of Armcx1 on the brains of mice after TBI, mice were injected with adeno-associated virus (AAV) specific to Armcx1 stereologically (Fig. S2a and b), as described above, which was followed by CCI to establish a mouse model of TBI. Next, western blot, immunofluorescence staining, and neurobehavioral evaluation were performed. There were three groups of knockdown viruses. First, fluorescence microscopy was used to verify the transfection effect of AAV (Fig. S3a). Then, western blot was used to identify the group with a better knockdown effect for use in

subsequent experiments (Fig. S3b and c). Compared to the sham group, the levels of Armcx1 protein in the brain of mice in the CCI group, the over-NC group and the sh-NC group were significantly decreased, which was recovered in the over-Armcx1 group and further decreased in the sh-Armcx1 group (Fig. 3a and b). Immunofluorescence results showed that the decreased fluorescence intensity of Armcx1 in the CCI group was partially recovered in the overexpression group, especially in axons. In the knockdown group, the protein fluorescence intensity decreased further (Fig. 3c and d). This verified the above trend of Armcx1 protein in western blot.

To determine the effects of Armcx1 on neurobehavioral performance in post-TBI mice, we assessed behavioral activity using three methods. All mice were trained for 3 days before these tests. Firstly, mNSS was used to evaluate the degree of neurological impairment in mice at different time points (Fig. 3e). Before CCI, the score of each group was 0. The scores of mice in the over-Armcx1 group were significantly lower than those of the over-NC group on days 3, 5, and 7 after CCI, indicating that the neurological deficits of mice in the group were recovered to some extent. The scores of the sh-Armcx1 group were higher than those of the sh-NC group, indicating more serious neurological deficits. Next, the adhesive removal test was adopted to evaluate the sensorimotor function of the mice (Fig. 3f and g). In the overexpression group, the latency before contact and the time taken for the mice to remove the tape from their forepaws were significantly shortened, while in the knockdown group, these indicators were prolonged to varying degrees. We also assessed the motor activity of mice after CCI using a rotarod test (Fig. 3h). Compared to the vector group, the over-Armcx1 group animals were able to spend more time on the rotarod, while the sh-Armcx1 group did the opposite. In the above tests, no significant difference was observed in the sham group at different time points, and no significant difference was found between the CCI group and the vector treatment groups. These results indicated that overexpression of Armcx1 rescued sensorimotor function deficit in mice to a certain extent; in contrast, knockdown of Armcx1 aggravated the sensorimotor function impairment in these animals.

Upregulation of Armcx1 rescued neuronal apoptosis, which was aggravated in the knockdown group

To evaluate the effects of overexpression and knockdown of Armcx1 on cell apoptosis in CCI mice, several apoptosis-related indicators were detected by western blot. Armcx1 is located on mitochondria and is closely associated with mitochondrial transport[18]. Recent studies have shown that caspase-9 is specific to the apoptosis of the mitochondrial pathway, and its degree of cleavage reflects the degree of pathway activation[28]. Both Bcl-2 and Bax belong to the Bcl-2 family and play a crucial role in the mitochondrial apoptosis pathway[29].

Western blotting was performed for cleaved caspase-9, Bax, and Bcl-2. As shown in Fig. 4a, b, and d, cleaved caspase-9 and Bax levels were significantly increased in the model group compared to the sham group, and this increase was partially recovered in the over-Armcx1 group. In the knockdown group, there was a slight increase in the expression level of cleaved caspase-9 and Bax compared to the negative control group, but the difference was not statistically significant. Bcl-2 levels showed the opposite trend in that they demonstrated a significant decrease after CCI, which was partially reversed in the

overexpression group. However, a significant decrease in Bcl-2 was observed in the knockdown group (Fig. 4a and c). These results suggest that overexpression of Armcx1 rescues the elevation of pro-apoptotic protein level, while knockdown of Armcx1 may play an opposing role. Therefore, Armcx1 is likely to play a neuroprotective role through an anti-apoptotic manner.

Overexpression of Armcx1 alleviates axonal injury and knockdown aggravates this phenomenon

We evaluated the effects of overexpression and silencing of Armcx1 on the ultrastructure of the ROI tissues in CCI mice by TEM (Fig. 5a). The axons in the sham group were smooth and full, and the myelin sheath was compact and uniform. Mitochondria in the cell bodies and axons have a regular round or oval shape. The inner membrane is highly folded and protrudes inward to form the crest. The outer membrane is uniform and completely covers the organelle. In the CCI group, as well as the NC group, the neuronal axons were irregular in shape, oblong, or fusiform, and the myelin sheaths were stratified and varied in density. The mitochondrial morphology of the cell body and axon was swollen and vacuolated, and the integrity of the mitochondrial crest and membrane was impaired. In the over-Armcx1 group, the morphology of the neuronal axons was similar to that of the sham group: the axons were oval, full in shape, and the myelin sheath was dense and uniform. The stratification was significantly improved compared to the carrier group. However, the ultrastructure of neurons in the knockdown group was similar to that in the CCI group, with irregular axon morphology, a stratified myelin sheath, and varying degree of density. Mitochondria in the axons and cell bodies were swollen and obviously vacuolated.

Studies have shown that TBI can induce excessive production of beta-amyloid precursor protein (β-APP), a marker of axonal degeneration[30]. Therefore, immunohistochemical staining of β-APP was performed to further assess the extent of axon damage (Fig. 5b and c). The results showed that β-APP accumulation in the area of interest was significant in the TBI group, which was significantly improved in the overexpression group, while in the knockdown group, the accumulation was even greater.

These data suggest that upregulation of Armcx1 contributes to the alleviation of the extent of axon damage, which may be attributed to improved mitochondrial status, as we saw healthier mitochondria (morphologically, at least) in the cell bodies and axons in the overexpression group, which is consistent with previous studies[18].

MiR-223-3P directly inhibits Armcx1

As the above experiments showed that Armcx1 has explicit neuroprotective effects, we next sought to determine its potential upstream regulatory factor(s). As predicted by TargetScanMouse7.2 and TargetScanHuman7.2 databases, miR-223-3P may bind to Armcx1. MiR-223-3P is a 22 bp non-coding RNA that binds to the 3'UTR of Armcx1 mRNA. The potential binding sequence of the 3'UTR of Armcx1 mRNA is 5'-AACTGACA-3', which may bind to the sequence of 5'-UGUCAGUU-3' in miR-223-3P (Fig. 6a). To confirm the assumption above, a dual-luciferase reporter gene assay was performed. The wild-type 3′UTR or mutant 3′UTR of Armcx1 mRNA was ligated downstream of the firefly luciferase gene in the pmirGLO plasmid (Promega) to generate Armcx1-3′UTR and Armcx1-3′mUTR plasmids. The Armcx1-

3′UTR and Armcx1-3′mUTR plasmids were cotransfected with miR-NC or miR-223-3P mimics into 293 T cells. The luciferase activity results showed that the luciferase activity of 293 T cells cotransfected with miR-223-3P mimics and Armcx1-3′UTR was obviously reduced. However, the luciferase activity of 293 T cells cotransfected with miR-223-3P mimics and Armcx1-3′mUTR was not changed significantly (Fig. 6b). These findings indicate that the 3'-UTR of Armcx1 is a direct target of miR-223-3P.

MiR-223-3P inhibits neurite extension without affecting neuronal branching

To further clarify the role of miR-223-3P in TBI, we transfected miR-223-3P mimic, miR-223-3P inhibitor, and the corresponding negative control oligonucleotides into primary cortical neurons from mice embryos. An in vitro scratch assay was established on this basis, which was followed by western blot and dual immunofluorescence. Western blot results showed that the level of Armcx1 protein decreased significantly in the scratch group compared to the control group. Furthermore, the Armcx1 protein level in the miR-223-3P mimic group was significantly lower than that in mimic-NC group, while the miR-223-3P inhibitor group showed an opposite trend (Fig. 6c and d); this once again confirmed the inhibitory effect of miR-223-3P on Armcx1. Statistical results of immunofluorescence further confirmed the western blotting results (Fig. 6e and f). Additionally, we quantified the total length of neurites and the number of branches by β3-tubulin staining to identify the role of miR-223-3P in axonal injury in the scratching model. Statistical results showed that the total length of neurites in the scratch group was lower than that in the control group. On this basis, the total length of neurites in the miR-223-3P mimic group was further decreased, which was significantly reversed in the miR-223-3P inhibitor group (Fig. 6g). In contrast, there was no significant difference in the number of branches among groups (Fig. 6h). Thus, it can be concluded that miR-223-3P inhibits the extension of neurites in the in vitro scratch model, without influencing the neuronal branching, which is probably achieved indirectly by negatively regulating Armcx1.

Effects of miR-223-3P mimics or inhibitor on scratch-induced mitochondrial dysfunction in cultured primary cortical neurons

To determine the effect of targeted inhibition of miR-223-3P on Armcx1 on mitochondrial function, we analyzed the MMP in scratch-treated primary cortical neurons using JC-1 staining (Fig. 7a).

JC-1 is an ideal fluorescent probe that is widely used to detect MMP. When the MMP of the cell is high, JC-1 dye aggregates in the matrix of mitochondria and forms J-aggregates, which produce red fluorescence. When the potential is low, the dye cannot aggregate in the matrix of mitochondria and the JC-1 dye exists as monomers, presenting as green fluorescence. Therefore, the change in MMP can be easily detected by the change in fluorescence color. The ratio of red to green fluorescence is often used to measure the proportion of mitochondrial depolarization. The ratio of red to green fluorescence depends only on MMP, but not on other factors[31].

In the control group, the axonal mitochondria were marked by strong red fluorescence of JC-1, while the green signal was barely detected, indicating good MMP. However, in the cell body, both red and green

fluorescent spots were observed, indicating the coexistence of healthy and damaged mitochondria. In sharp contrast, red JC-1 fluorescence was significantly decreased in the cell body and axon of neurons in the scratch group, and strong green fluorescence was clearly seen. The fluorescence changes in JC-1 from red to green indicate the loss of MMP in these cells. In the miR-223-3P mimic group, the red fluorescence in both cell bodies and axons got further weakened, while the green fluorescence was further enhanced, indicating further loss of overall MMP. This trend was partially reversed in the miR-223-3P inhibitor group, suggesting an overall robust MPP. There was no significant difference in the red-green fluorescence ratio between the negative control and scratch groups. Quantitative analysis further verified the morphological observations above (Fig. 7b). These results suggest that miR-223-3P inhibits MMP, either by directly weakening the potential difference between mitochondrial inner membrane and outer membrane (e.g., by calcium influx) or by regulating the distribution of healthy and damaged mitochondria.

Discussion

In TBI, damaged mitochondria are present in the cell bodies and axons of neurons. The clearance of damaged neurons and the replenishment of healthy mitochondria are key to maintaining the normal function of neurons[12]. Damaged mitochondria are transported to the cell body for degradation through mitochondrial autophagy, and healthy mitochondria generated in the soma are transported to the distal end to meet the increased energy demand, both of which require enhanced mitochondrial transport[13]. The distribution of mitochondria in neurons, especially in axons, is coordinated by microtubule-based transport mechanisms powered by ATP hydrolysis. This involves a series of transport-related proteins, including kinesin, dynein, Trak1/2, and Miro1/2. The kinesin-1 family are major motors that drive neuronal mitochondria along microtubules to their distal axons and synapses. Dynein is the main driving force for microtubule-based retrograde transport. In mammalian cells, two Trak proteins guide mitochondrial polarized transport, each playing different roles: Trak1 is mainly distributed in the axon and binds to both kinesin-1 and dynein, and is required for axon localization of mitochondria, while Trak2 is mainly localized in dendrites and primarily interacts with dynein, which is responsible for the dendritic distribution of mitochondria. Miro binds to a motor adapter, Trak1/2, to bind kinesin-1 and dynein motors to the mitochondrial surface indirectly. Two Miro homologue proteins exist in mammalian cells, Miro-1 and Miro-2, and share 60% of the same sequence[8, 32–37]. Elevated Miro1 expression recruits more Trak and motor proteins, enhancing mitochondrial transport[38, 39]. Drosophila dMiro helps to regulate anterograde and retrograde mitochondrial transport on axons[40], while dMiro or Miro-1 deletion in mouse cortical neurons impairs retrograde mitochondrial transport[40, 41]. In 2016, Cartoni et al. found that Armcx1 locates on neuronal mitochondria and interacts with Miro1. Overexpression of Armcx1 enhances neuronal mitochondrial transport by recruiting resting mitochondria into motor cisterns and promotes the survival and axonal growth of axon-cut retinal ganglion cells, while inhibition of Armcx1 expression has the opposite effect[18]. Therefore, we were inspired to explore the protein further in a mouse CCI model, which, to the best of our knowledge, is the first report of Armcx1 being studied in a TBI model.

In this experiment, we first found that the expression of Armcx1 in the parietal lobe tissue was high in mice in the sham group. In the CCI group, the expression level of Armcx1 in the tissues around the impact decreased gradually to the lowest level 3 days after CCI, and then increased slowly. By immunofluorescence, we found that Armcx1 was mainly expressed in neurons compared to astrocytes and microglia, which was consistent with the findings of a previous study. Therefore, in the next experiment, we focused on neurons 3 days after CCI to further explore the role of Armcx1.

In our second experiment, Armcx1 was upregulated and suppressed by injection of Armcx1-specific overexpression and knockdown adeno-associated viruses into the right parietal cortex stereotypically. Firstly, the expression level of Armcx1 was detected by western blot to ensure the successful transfection of *Armcx1* and the effective regulation of Armcx1 protein level. Subsequently, the sensorimotor function of each group was evaluated by the mNSS, adhesion test, and rotarod test. The results showed that overexpression of Armcx1 significantly eased CCI-induced sensory and motor dysfunction, which were exacerbated by knockdown of Armcx1 via injection of AAV-hSYN-shRNA (Armcx1).

The exciting findings above led us to wonder whether Armcx1 affects apoptosis, which is always accompanied by the occurrence of TBI. Caspase-9 is activated during apoptosis and is a key factor in mitochondrial pathway apoptosis. The pro-apoptotic protein Bax and the anti-apoptotic protein Bcl-2 also play important roles in this process[42, 43]. The results of western blot showed that cleaved caspase-9 and Bax protein levels were significantly increased and Bcl-2 was significantly decreased after CCI. Moreover, overexpression of Armcx1 partially reversed the above trend, while knockdown of Armcx1 showed opposite results. These results indicated that elevated Armcx1 expression could inhibit apoptosis after TBI.

We then observed the ultrastructure of neurons using TEM to evaluate whether Armcx1 affects axonal injury. It was found that upregulation of Armcx1 significantly eased distal axonal injury after TBI, while inhibition of Armcx1 expression intensified these injuries. Axonal degeneration after TBI significantly increases the production of β-APP, a sign of complete axonal disconnection[30]. Immunohistochemistry showed β-APP accumulation was significantly reduced in the overexpression group and increased in the knockdown group, indicating that overexpression of Armcx1 alleviated axonal injury. Excitingly, TEM also showed that the morphology of damaged mitochondria in the soma and axons of neurons in Armcx1 overexpression mice was evidently improved after CCI, but not in the knockdown group. This implies that the overexpression of Armcx1 enhances mitochondrial status, which is likely achieved by promoting microtubule-based bidirectional transport of damaged and healthy mitochondria in axons. Of course, this improvement could be achieved by other means, but so far, no such studies have been reported.

MiRNAs are a class of small non-coding RNAs that regulate gene expression at the post-transcriptional level and play an important role in maintaining and regulating physiological functions. Notably, studies have shown changes in miRNA levels in the cerebral cortex and hippocampus in rats and mice after TBI. These miRNAs may promote or inhibit the formation of secondary brain injury via apoptosis, neuronal repair, blood-brain barrier leakage, and inflammatory responses[22, 44]. MiR-223-3P is a hematopoietic

related miRNA that affects hematopoietic cell differentiation, activation, and inflammatory response[20]. Additionally, miR-223-3P is also expressed in the brain, and studies have shown that its expression is increased in the cortex and hippocampus after TBI[21–23]. Bioinformatics predicted that miR-223-3P has the potential to inhibit Armcx1 (TargetScanMouse7.2). To verify this, in the third experiment, we first performed a double luciferase reporter gene assay. The results confirmed our hypothesis that miR-223-3P directly inhibited mRNA expression by targeting its 3'UTR region. Next, cultured mouse cortical neurons were transfected with miR-223-3P mimic and inhibitor in vitro. The results of western blot and immunofluorescence further confirmed the inhibitory effect of miR-223-3P on Armcx1. Meanwhile, we also found that the total length of neurites in the miR-223-3P mimic group was significantly shortened, which was reversed in the miR-223-3P inhibitor group. Interestingly, there was no significant difference in the number of branches of these neurons, which seems to suggest a change in the average length of those neurites. Generally, neurons contain one axon and several dendrites. Whether the change in the total length of neurites is caused by axon lengthening, dendrite lengthening, or both, is an interesting question, which remains to be determined. As miR-223-3P inhibits the expression of Armcx1 after injury, we questioned whether miR-223-3P affects mitochondrial status. To this end, MMP was detected by JC-1 staining. Surprisingly, the MMP in the miR-223-3P mimic group was significantly lower than that in the control group, while mitochondria in the miR-223-3P inhibitor group were in a relatively healthy state of depolarization. This suggests that miR-223-3P has remarkably adverse effects on the status of neuronal mitochondria. The direct inhibitory effect of miR-223-3P on Armcx1 and the results of our in vivo experiments suggest that elevated miR-223-3P aggravates secondary injury after TBI, potentially by downregulating the expression of Armcx1 and inhibiting mitochondrial transport (Fig. 8). As how the interaction between Armcx1 and Miro1 regulates mitochondrial transport along the microtubule is still unknown, further studies are needed to uncover the mechanisms involved.

Previous studies have found that miR-223-3P appears to promote neural repair and regeneration. In a mouse model of cerebral ischemia, miR-223$^{-/-}$ mice showed deficits in context memory, enhanced excitatory toxicity, and neuronal death. In contrast, miR-223 overexpression inhibits NMDA-induced calcium influx in hippocampal neurons by targeting GluR2 and NR2B, and protects neurocytes from death following transient global cerebral ischemia and excitatory injury[21]. Another study showed that overexpression of miR-223 in the retina and optic nerve prevented the formation of EAE-driven pathological axon swelling, due to reduced excitatory toxicity by inhibiting GluR2 and NR2B expression[45]. Taken together, these results suggest that miR-223-3P plays distinct roles in neuronal response to injury, which may be vary according to the experimental species, cell type, injury mode, occurrence site, and injury time.

This study has some limitations. First, healthy adult male C57BL/6 mice were used to establish the CCI model by pneumatic impactor devices; however, this does not fully recapitulate the clinical process of TBI, such as traffic accident, accidental fall, and impact by hard objects. Additionally, the role of Armcx1 in each sex needs to be evaluated in further studies. Second, in clinical practice, drugs are often administered orally or intravenously, but considering the metabolism and absorption of Armcx1 in the

digestive system and circulatory system, we chose exogenous adeno-associated virus transduction through the cortex injection to elevate the function of Armcx1. Third, we only studied the effects of Armcx1 on apoptosis and axonal injury after TBI, and the role of Armcx1 in other secondary injury responses such as excitatory toxicity, oxidative stress, and the inflammatory response, remains unclear. Fourth, how changes in the expression of Armcx1 affect its interaction with Miro1, and whether it induces an increase in Miro1 expression or just increases the proportion of the two bindings remains unknown. Fifth, the expression of miR-223-3P and its relationship with Armcx1 in TBI animal models have not been reported. Therefore, much work remains to be done to understand the role of miR-223-3P/Armcx1 in TBI. Fortunately, current work suggests that this approach has good therapeutic potential for TBI. Although it will take some time for the clinical application of Armcx1, we will continue to conduct in-depth research to promote the early realization of its clinical application.

Conclusion

TBI is one of the leading causes of death and disability worldwide, and current treatment results are far from satisfactory[46, 47]. There is an urgent need for more effective treatments to minimize secondary brain damage from TBI. Using a clinically relevant mouse CCI model, we explored a novel neuroprotective strategy targeting Armcx1. After CCI, the decrease in Armcx1 expression was found to aggravate apoptosis and axonal injury and lead to further aggravation of neurological dysfunction. Exogenous Armcx1 could reduce mitochondrial and axonal injury, save cells from apoptosis, alleviate the secondary injury of TBI, and bring favorable neurological prognosis. Additionally, we verified the direct inhibition of miR-223-3P on Armcx1 in in vitro experiments. Exogenous miR-223-3P treatment promoted the prolongation of neurites and the improvement of MMP. Therefore, miR-223-3P/Armcx1 may be a promising target for TBI therapy.

Declarations

Acknowledgments

We would like to express our sincere gratitude to Researcher Haiying Li (Department of Neurosurgery & Brain and Nerve Research Laboratory, The First Affiliated Hospital of Soochow University) for her patient guidance and help throughout this experiment. We also want to thank our family, friends and schoolmates for their care and encouragement during the experiment. Finally, we thank LetPub (www.letpub.com) for its linguistic assistance during the preparation of this manuscript.

Funding

This work was supported by the National Natural Science Foundation of China (No. 81971171) and Suzhou Science and Technology Project (No. SLT201906).

Competing Interests

The authors have no relevant financial or non-financial interests to disclose.

Author contributions

Dengfeng Lu: methodology, investigation and original draft writing. Yi Wang: software, data collection and analysis. Guangjie Liu: data collection, visualization. Shixin Wang: software, statistical analysis. Jing Wang: conceptualization. Yu Wu: writing, reviewing, editing. Xiaoou Sun: writing, reviewing, editing, resources, project administration and funding acquisition. All authors read and approved the final manuscript.

Data Availability

The data that support the findings of this study are available from the corresponding author upon reasonable request.

Ethics approval

All of the procedures were approved by the Ethics Committee of the First Affiliated Hospital of Soochow University and conformed to the Animal Research: Reporting In Vivo Experiments (ARRIVE) guidelines.

Consent to participate

Not applicable.

Consent for publication

Not applicable.

References

1. Rosenfeld JV et al (2012) Early management of severe traumatic brain injury. Lancet (London, England) 380(9847):1088–1098
2. Jiang J-Y et al (2019) Traumatic brain injury in China. Lancet Neurol 18(3):286–295
3. Werner C, Engelhard K (2007) Pathophysiology of traumatic brain injury. Br J Anaesth 99(1):4–9
4. LaPlaca MC et al (2007) CNS injury biomechanics and experimental models. Prog Brain Res 161:13–26
5. Wang Z-G et al (2016) bFGF Protects Against Blood-Brain Barrier Damage Through Junction Protein Regulation via PI3K-Akt-Rac1 Pathway Following Traumatic Brain Injury. Mol Neurobiol 53(10):7298–7311
6. Carteri RB et al (2019) Testosterone Administration after Traumatic Brain Injury Reduces Mitochondrial Dysfunction and Neurodegeneration. J Neurotrauma 36(14):2246–2259

7. Aubrecht TG et al (2018) Comparing effects of CDK inhibition and E2F1/2 ablation on neuronal cell death pathways in vitro and after traumatic brain injury, vol 9. Cell death & disease, p 112111
8. Lin M-Y, Sheng Z-H (2015) Regulation of mitochondrial transport in neurons. Exp Cell Res 334(1):35–44
9. Guo X et al (2005) The GTPase dMiro is required for axonal transport of mitochondria to Drosophila synapses. Neuron 47(3):379–393
10. Verstreken P et al (2005) Synaptic mitochondria are critical for mobilization of reserve pool vesicles at Drosophila neuromuscular junctions. Neuron 47(3):365–378
11. Stowers RS et al (2002) Axonal transport of mitochondria to synapses depends on milton, a novel Drosophila protein. Neuron 36(6):1063–1077
12. Zhou B et al (2016) Facilitation of axon regeneration by enhancing mitochondrial transport and rescuing energy deficits. J Cell Biol 214(1):103–119
13. Salinas S, Bilsland LG, Schiavo G (2008) Molecular landmarks along the axonal route: axonal transport in health and disease. Curr Opin Cell Biol 20(4):445–453
14. Lin MT, Beal MF (2006) Mitochondrial dysfunction and oxidative stress in neurodegenerative diseases. Nature 443(7113):787–795
15. Chan DC (2006) Mitochondria: dynamic organelles in disease, aging, and development. Cell 125(7):1241–1252
16. Stokin GB, Goldstein LSB (2006) Axonal transport and Alzheimer's disease. Annu Rev Biochem 75:607–627
17. Hirokawa N, Takemura R (2004) Kinesin superfamily proteins and their various functions and dynamics. Exp Cell Res 301(1):50–59
18. Cartoni R et al (2016) The Mammalian-Specific Protein Armcx1 Regulates Mitochondrial Transport during Axon Regeneration. Neuron 92(6):1294–1307
19. Sabirzhanov B et al (2014) Downregulation of miR-23a and miR-27a following experimental traumatic brain injury induces neuronal cell death through activation of proapoptotic Bcl-2 proteins. The Journal of neuroscience: the official journal of the Society for Neuroscience 34(30):10055–10071
20. Juzwik CA et al (2019) microRNA dysregulation in neurodegenerative diseases: A systematic review. Prog Neurobiol 182:101664
21. Harraz MM et al (2012) MicroRNA-223 is neuroprotective by targeting glutamate receptors. Proc Natl Acad Sci U S A 109(46):18962–18967
22. Lei P et al (2009) Microarray based analysis of microRNA expression in rat cerebral cortex after traumatic brain injury. Brain Res 1284:191–201
23. Wang WX et al (2015) Mitochondria-associated microRNAs in rat hippocampus following traumatic brain injury. Exp Neurol 265:84–93

24. Cui W et al (2021) 20-HETE synthesis inhibition attenuates traumatic brain injury-induced mitochondrial dysfunction and neuronal apoptosis via the SIRT1/PGC-1alpha pathway: A translational study. Cell Prolif 54(2):e12964
25. Wu YH et al (2021) *In Vitro Models of Traumatic Brain Injury: A Systematic Review*.J Neurotrauma,
26. Bae YH et al (2018) Brain injury induces HIF-1alpha-dependent transcriptional activation of LRRK2 that exacerbates brain damage, vol 9. Cell death & disease, p 112511
27. Xu J et al (2020) IL-4/STAT6 signaling facilitates innate hematoma resolution and neurological recovery after hemorrhagic stroke in mice. Proc Natl Acad Sci U S A 117(51):32679–32690
28. Romero-Molina C et al (2018) Distinct Microglial Responses in Two Transgenic Murine Models of TAU Pathology. Front Cell Neurosci 12:421
29. Tan X et al (2020) Fibroblast Growth Factor 10 Attenuates Renal Damage by Regulating Endoplasmic Reticulum Stress After Ischemia-Reperfusion Injury. Front Pharmacol 11:39
30. Anthony Jalin AMA et al (2019) EPPS treatment attenuates traumatic brain injury in mice by reducing Abeta burden and ameliorating neuronal autophagic flux. Exp Neurol 314:20–33
31. Perry SW et al (2011) Mitochondrial membrane potential probes and the proton gradient: a practical usage guide. Biotechniques 50(2):98–115
32. Kruppa AJ, Buss F (2021) *Motor proteins at the mitochondria-cytoskeleton interface*.J Cell Sci, **134**(7)
33. Melkov A, Abdu U (2018) Regulation of long-distance transport of mitochondria along microtubules. Cell Mol Life Sci 75(2):163–176
34. Zhao Y et al (2021) Metaxins are core components of mitochondrial transport adaptor complexes. Nat Commun 12(1):83
35. Lopez-Domenech G et al (2018) Miro proteins coordinate microtubule- and actin-dependent mitochondrial transport and distribution. EMBO J 37(3):321–336
36. Mandal A, Drerup CM (2019) Axonal Transport and Mitochondrial Function in Neurons. Front Cell Neurosci 13:373
37. El-Hattab AW et al (2018) Mitochondrial dynamics: Biological roles, molecular machinery, and related diseases. Mol Genet Metab 125(4):315–321
38. Chen Y, Sheng ZH (2013) Kinesin-1-syntaphilin coupling mediates activity-dependent regulation of axonal mitochondrial transport. J Cell Biol 202(2):351–364
39. MacAskill AF et al (2009) GTPase dependent recruitment of Grif-1 by Miro1 regulates mitochondrial trafficking in hippocampal neurons. Mol Cell Neurosci 40(3):301–312
40. Russo GJ et al (2009) Drosophila Miro is required for both anterograde and retrograde axonal mitochondrial transport. J Neurosci 29(17):5443–5455
41. Nguyen TT et al (2014) Loss of Miro1-directed mitochondrial movement results in a novel murine model for neuron disease. Proc Natl Acad Sci U S A 111(35):E3631–E3640

42. Akamatsu Y, Hanafy KA (2020) Cell Death and Recovery in Traumatic Brain Injury. Neurotherapeutics 17(2):446–456
43. Deng H et al (2021) B-Cell Lymphoma 2 (Bcl-2) Gene Is Associated with Intracranial Hypertension after Severe Traumatic Brain Injury. J Neurotrauma 38(2):291–299
44. Pan YB, Sun ZL, Feng DF (2017) The Role of MicroRNA in Traumatic Brain Injury. Neuroscience 367:189–199
45. Morquette B et al (2019) MicroRNA-223 protects neurons from degeneration in experimental autoimmune encephalomyelitis. Brain 142(10):2979–2995
46. Feng J, Jiang J (2020) Traumatic brain injury in 2019: databases, biomarkers, and stratified treatment. Lancet Neurol 19(1):5–7
47. Lammy S (2020) *Management of traumatic brain injury in China versus Europe*.The Lancet Neurology, **19**(11)

Figures

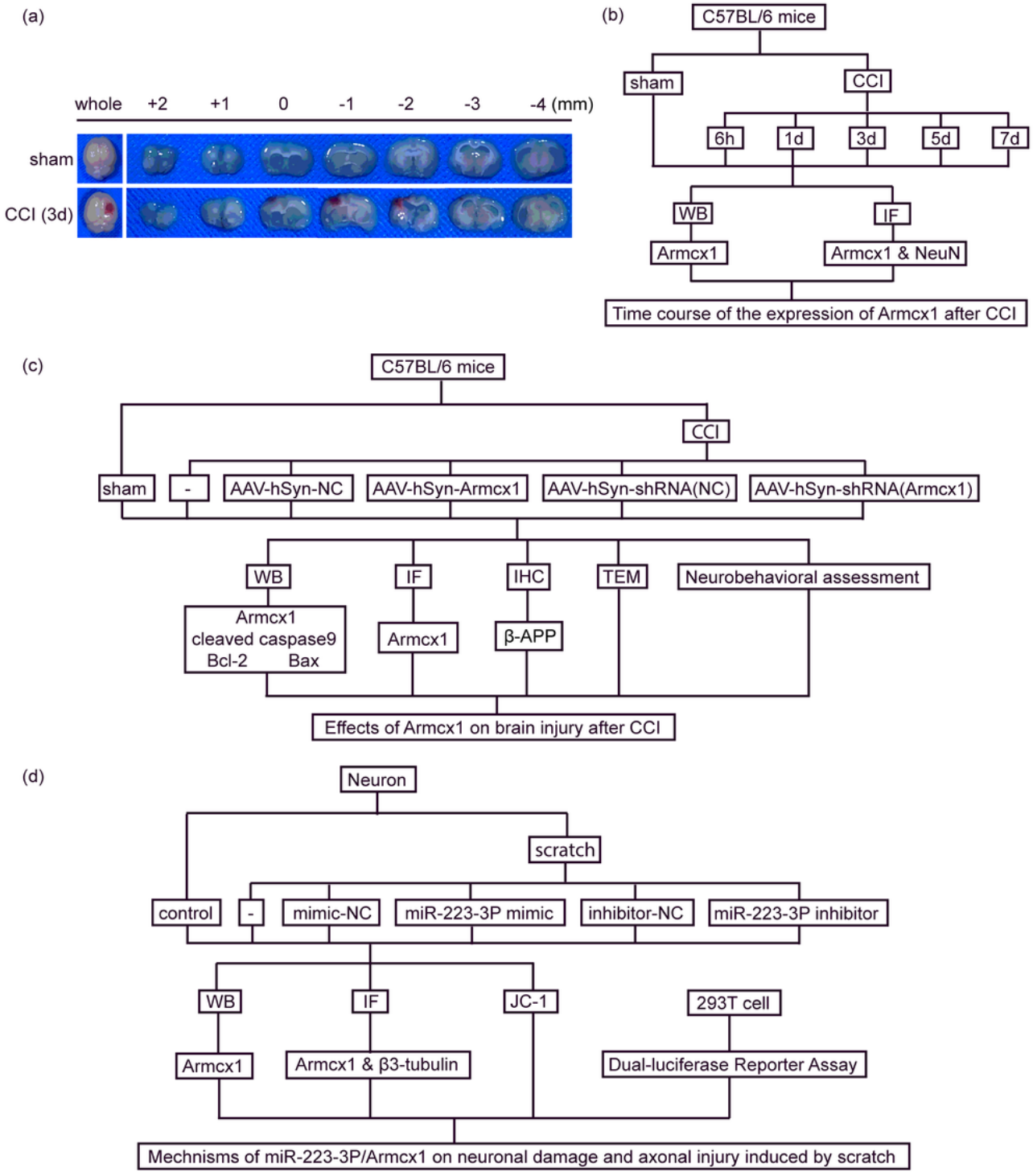

Figure 1

Mouse controlled cortical impact (CCI) model and experimental design. a Coronal sections of the brains from sham and CCI mice at 72 h. b Time course of Armcx1 protein levels in brain tissue around the contusion post-CCI. c, d The role of Armcx1 in CCI-induced secondary brain injury and its potential mechanism. CCI: controlled cortical impact; WB: western blot analysis; IF: immunofluorescent analysis; AAV: Adeno-associated virus; hSYN: human Synapsin I; NC: negative control; shRNA: short hairpin RNA;

IHC: immunohistochemistry analysis; TEM: transmission electron microscope; Bcl-2: B-cell lymphoma-2; Bax: Bcl2-associated X protein; β-APP: beta-amyloid precursor protein; JC-1: 5,5',6,6'-tetrachloro1,1',3,3'-tetramethylbenzimidazolylcarbocyanine iodide.

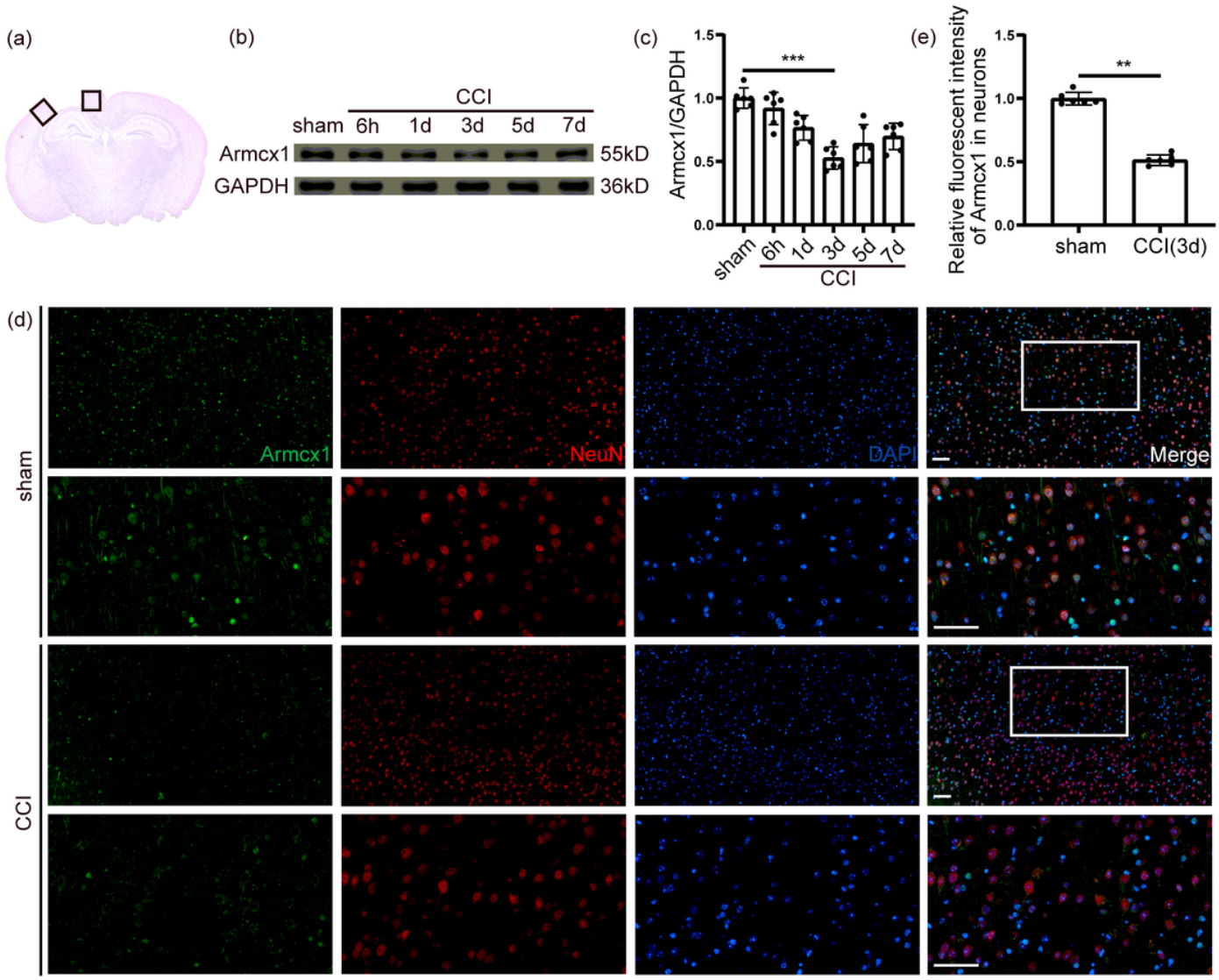

Figure 2

Protein level of Armcx1 in the CCI-induced peri-lesion brain tissue of mice. a The areas framed in black represent the representative cortical areas for the subsequent experimental procedures. b, c Western blotting and quantification of Armcx1 protein levels at specified time points in brain tissue around contusion. ***P < 0.001 vs. sham group, n = 6. d, e Dual immunofluorescence analysis was performed on brain slices with antibodies against Armcx1 (green) and neuron marker (NeuN, red). The nuclei were fluorescently labeled with DAPI (blue). Scale bar = 50 μm. The relative fluorescence intensity of Armcx1 in neurons is shown. **P < 0.01 vs. sham group, n = 6.

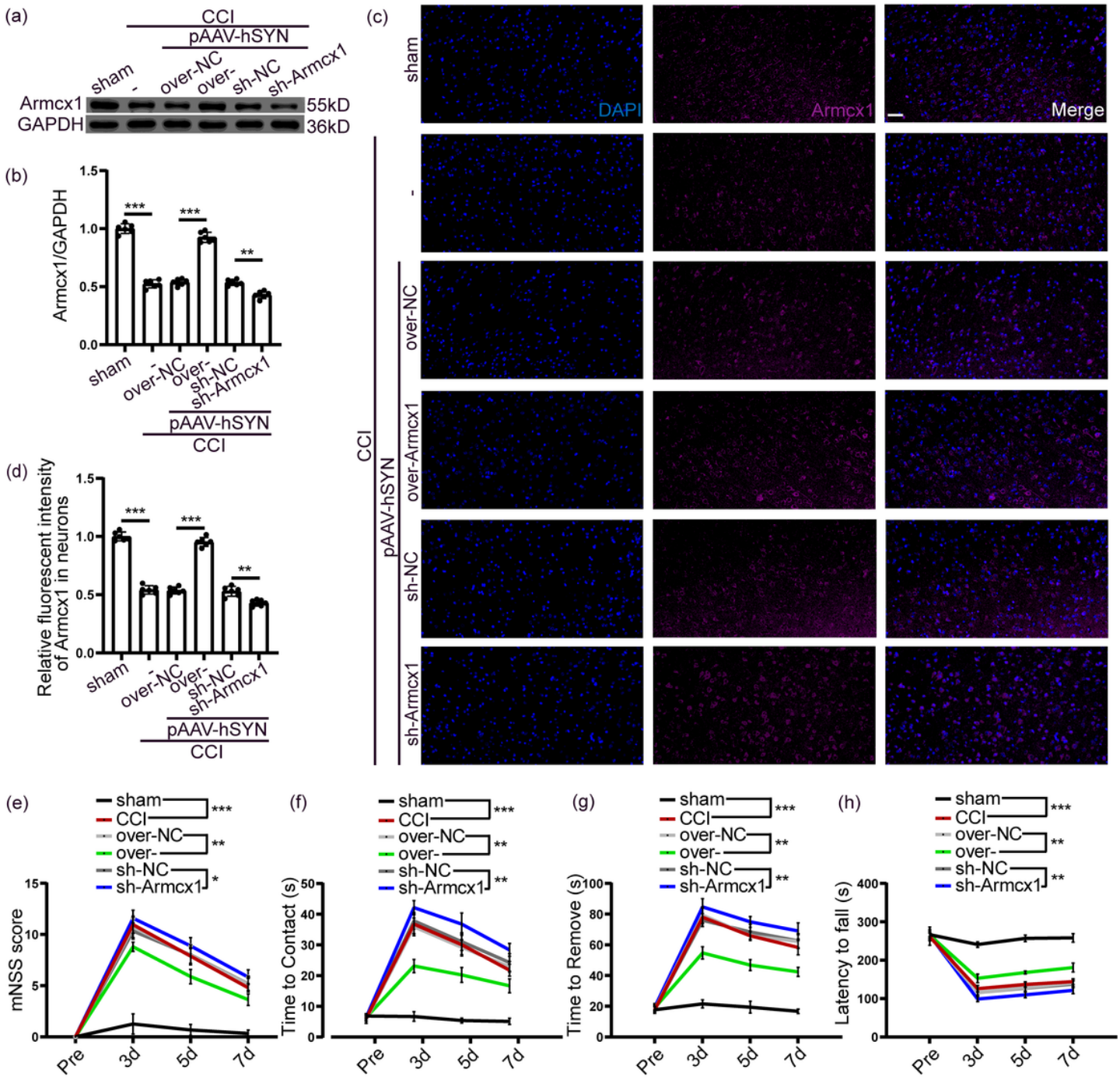

Figure 3

Overexpression and knockdown of Armcx1 and its effects on neurological recovery of mice after CCI. a, b Western blotting and quantification of Armcx1 protein levels in peri-contusion brain tissue with adeno-associated virus transfection at 72 h after CCI. ***P < 0.001 **P < 0.01, n = 6. c, d Immunofluorescence analysis was performed on brain slices with antibodies against Armcx1 (magenta). The nuclei were fluorescently labeled with DAPI (blue). Scale bar = 50 μm. The relative fluorescence intensity of Armcx1 in neurons is shown. ***P < 0.001, **P < 0.01, n = 6. e The Modified Neurological Severity Score (mNSS) was evaluated before and at 3, 5, and 7 days post-CCI. ***P < 0.001, **P < 0.01, *P < 0.05, n = 12. f Time to feel

the adhesive tapes in the adhesive removal test before and at 3, 5, and 7 days post-CCI. ***P < 0.001 **P < 0.01, n = 12. g Time to remove the adhesive tapes in the adhesive removal test before and at 3, 5, and 7 days post-CCI. ***P < 0.001, **P < 0.01, n = 12. h The latency to fall in the rotarod test before and at 3, 5, and 7 days post-CCI. ***P < 0.001, **P < 0.01, n = 12.

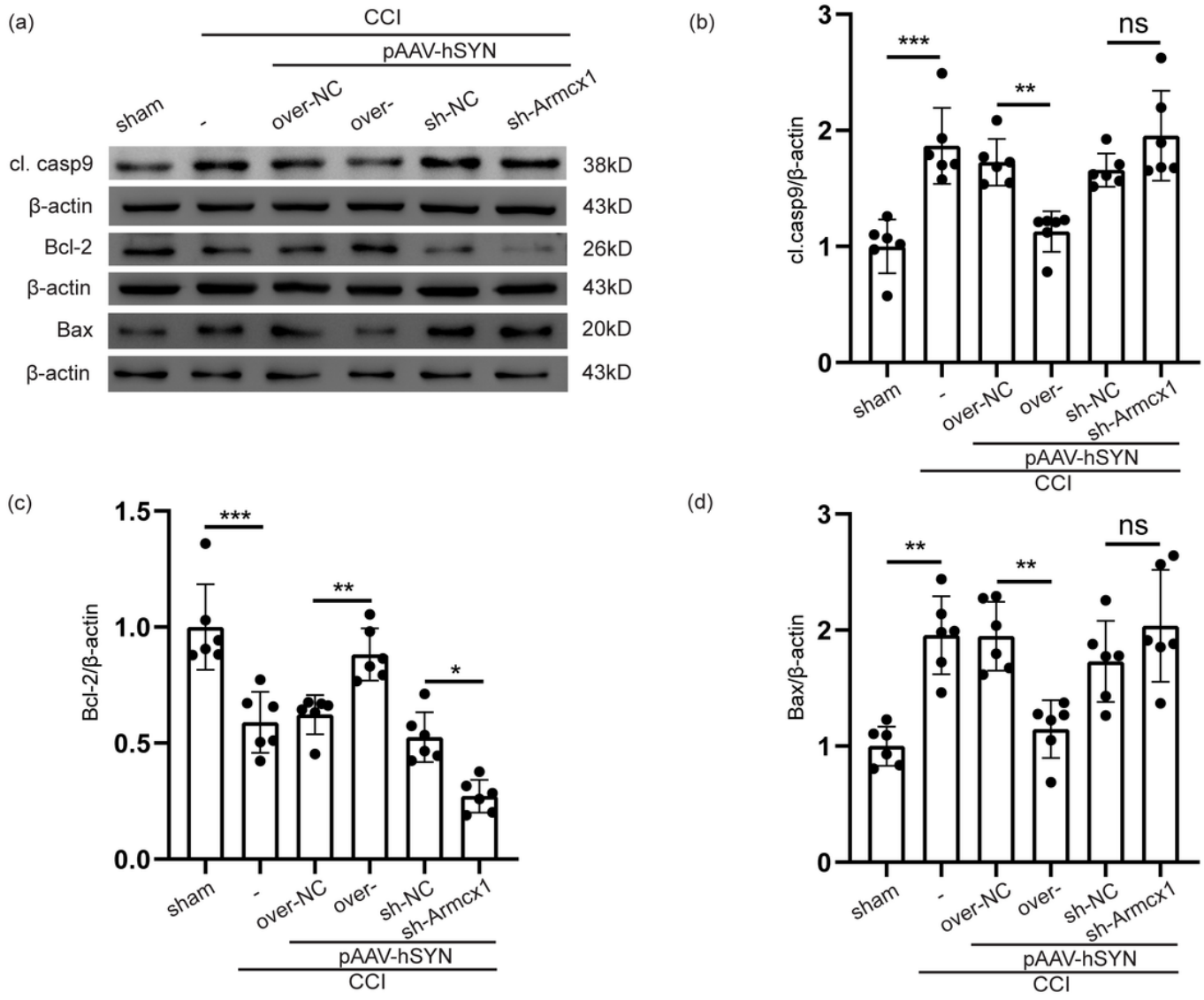

Figure 4

Overexpression and knockdown of Armcx1 on apoptosis in peri-lesion tissues in mice brains. a-d Western blotting and quantification of protein levels of cleaved caspase-9, Bcl-2, and Bax in peri-lesion tissue with adeno-associated virus transfection 72 h after CCI. ***P < 0.001 **P < 0.01, *P < 0.05, n = 6.

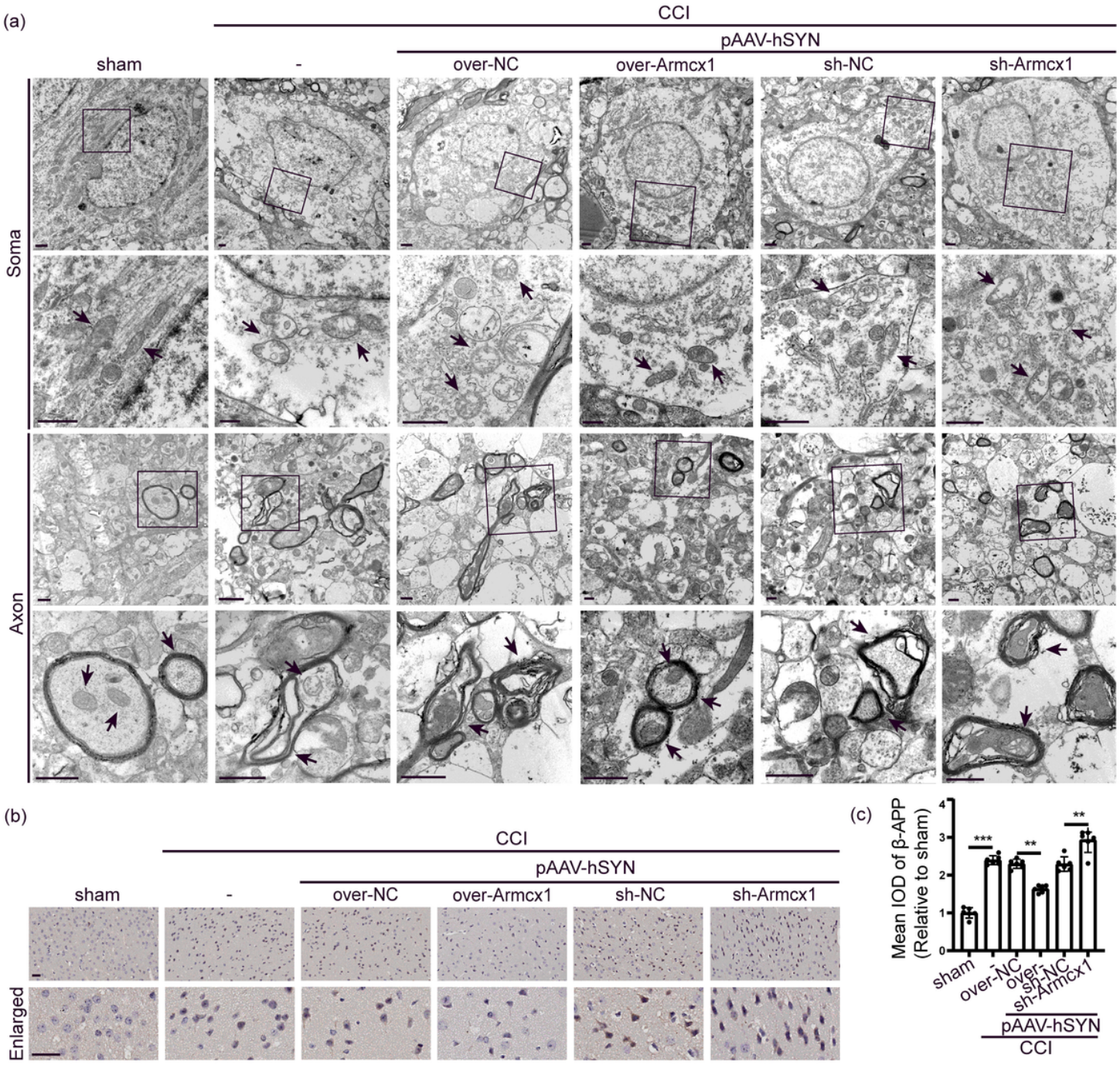

Figure 5

Effects of overexpression and knockdown of Armcx1 on neuronal ultrastructure and axonal injury in CCI mice. a Representative ultrastructure of neurons in each group, with normal and damaged mitochondria and distal axons indicated by arrows. Scale bar = 250 nm n = 3. b, c Immunohistochemistry analysis and quantification of β-amyloid precursor protein (β-APP) in peri-contusion brain tissue with adeno-associated virus transduction at 72 h after CCI. Scale bar = 50 μm. ***P < 0.001 **P < 0.01, n = 6.

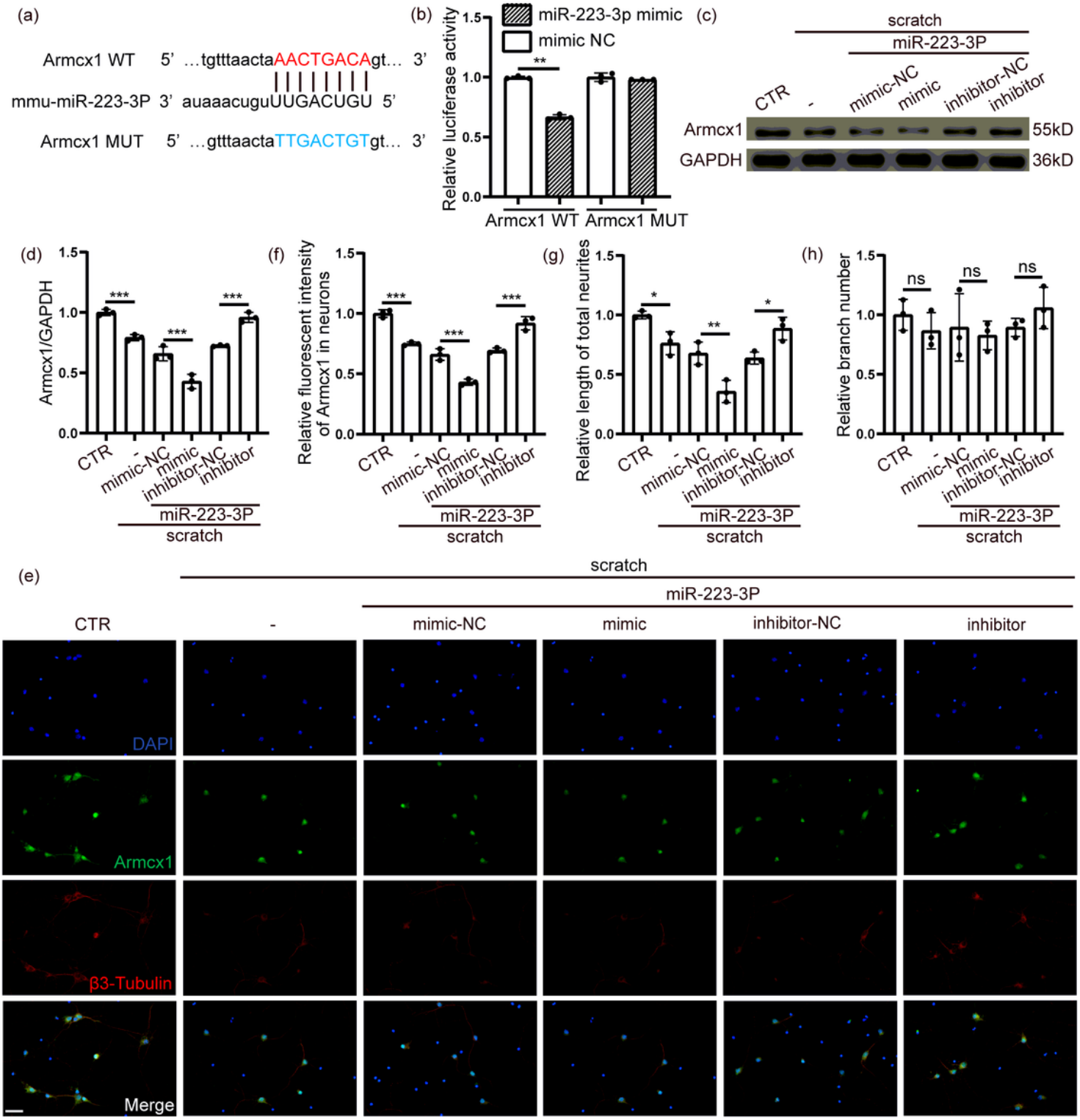

Figure 6

Effects of miR-223-3P on Armcx1 and total lengths of neurites and branch numbers. a mmu-miR-223-3p and Armcx1-3'UTR target binding sites and Armcx1 mutation sites. b Detection of mmu-miR-223-3P and Armcx1-3'UTR interaction by dual luciferase reporter assay. c, d Western blotting and quantification of Armcx1 protein levels in cultured neurons with either mmu-miR-223-3P mimic or inhibitor treatment 72 h after scratch. ***P < 0.001, n = 3. e, f Immunofluorescence analysis was performed with antibodies

against Armcx1 (green) and β3-tubulin (red) in cultured neurons 72 h after scratch. Nuclei were fluorescently labeled with DAPI (blue). Scale bar = 50 μm. The relative fluorescence intensity of Armcx1 in neurons is shown. ***P < 0.001, n = 3. g The total length of neurites labeled with β3-tubulin (red) was calculated. **P <0.01, *P < 0.05, n = 3. h The branch numbers of cultured neurons were calculated. n = 3.

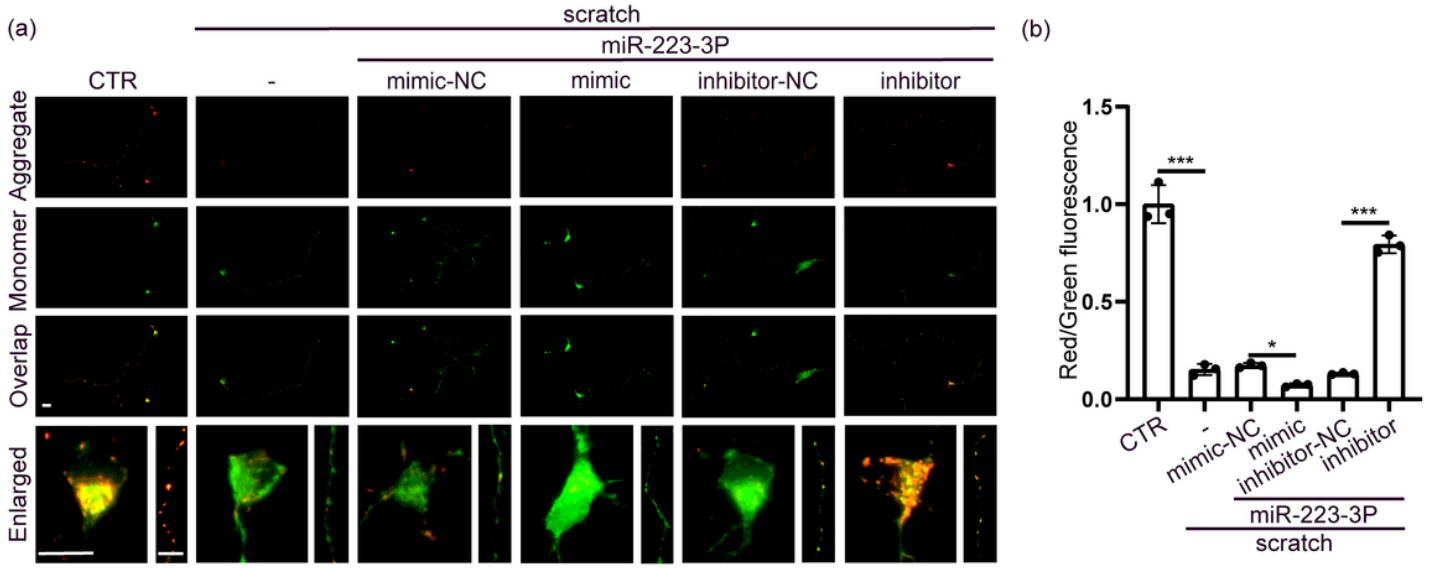

Figure 7

Effects of miR-223-3P on mitochondrial membrane potential (MMP) in the soma and axons of cultured neurons 72 h after scratch. a Representative images of JC-1 staining showing red fluorescence of JC-1 aggregate and green signal of monomer. Scale bar: 20 μm. b Quantification of the ratio of red to green fluorescence. ***P < 0.001, *P < 0.05 vs. control group, n = 3.

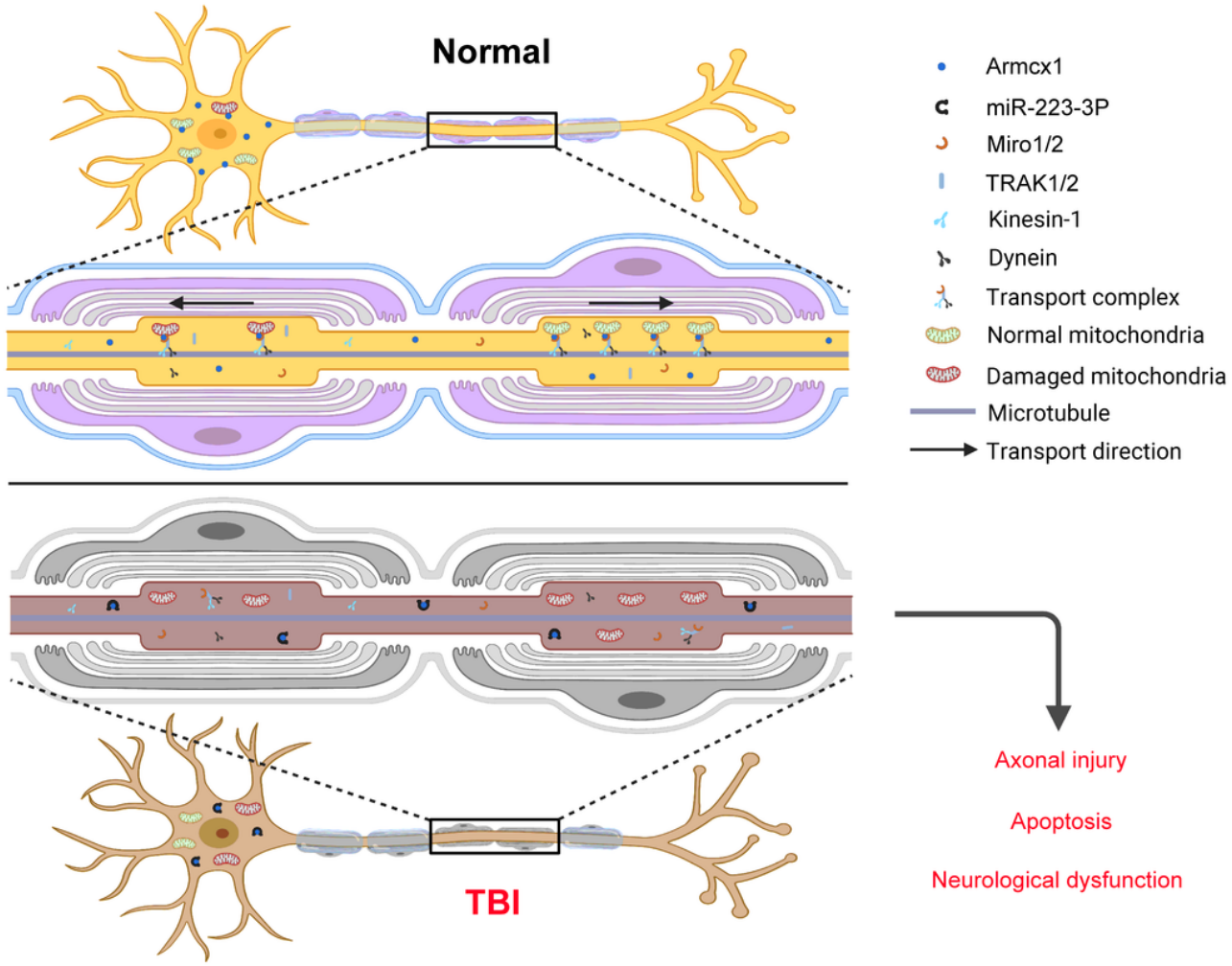

Figure 8

Schematic representations of the potential mechanisms of miR-223-3P/Armcx1 in traumatic brain injury (TBI).

Supplementary Files

This is a list of supplementary files associated with this preprint. Click to download.

- OnlineFigS1.png
- OnlineFigS2.png
- OnlineFigS3.png